Excellent Performance in Lithium-Ion Battery Anodes: Rational Synthesis of $Co(CO_3)_{0.5}(OH)0.11H_2O$ Nanobelt Array and Its Conversion into Mesoporous and Single-Crystal Co_3O_4

Yu Wang,[†,]* Hui Xia,[‡] Li Lu,[‡] and Jianyi Lin[†,]*

[†]Institute of Chemical and Engineering Sciences (ICES), 1, Pesek Road, Jurong Island, Singapore 627833 and [‡]Department of Mechanical Engineering, National University of Singapore, Singapore 117576

ABSTRACT Herein, we report a rational method to synthesize a Co_3O_4 nanobelt array on a conducting substrate and functionalize it in the application of Li-ion battery anodes, which is a novel and facile approach to access the nanobelt array of transition metal oxides. Compared to the previous reports, the as-prepared samples in our experiments exhibited both mesoporosity and single-crystallinity, and meanwhile, good contact with the conducting substrate (*via* a thin layer of TiO_2) provided an express pathway for charge transfer when they were applied in Li-ion batteries without any need to add other ancillary materials (carbon black or binder) to enhance the system's conductivity and stability. Under the condition of high charge—discharge current density of 177 mA/g in Li-ion batteries' testing, the Co_3O_4 nanobelt array was capable of retaining the specific capacity of 770 mAh/g over 25 cycles. Moreover, even though the charge—discharge rates were increased to 1670 and 3350 mA/g, it still could have reached the stable retention of the specific capacity of 510 and 330 mAh/g beyond 30 cycles, respectively, indicating an obtainable excellent rate capability. More importantly, the improved performance in Li-ion battery testing was definitely ascribed to the unique structures in our samples after elaborate analysis. So the final conclusion would be given that the lab-synthesized Co_3O_4 nanobelt array potentially could be a highly qualified candidate for Li-ion battery anodes in some practical fields, where high capacity and good capability are strictly required.

KEYWORDS: nanobelt array · mesoporous · lithium-ion batteries · capacity · capability

Electrochemical energy storage devices, which typically include lithium-ion batteries and supercapacitors, have drawn worldwide interests since the realization of the energy crisis.[1−7] Among all materials applicable for Li-ion battery anodes, transition metal oxides have always been regarded as the more promising candidates due to their relatively low cost, environmental benignity, higher theoretical capacity, and safety during operations.[8−10] Concerning their applications, additional emphasis is imposed on three particular parameters, namely, surface area, monocrystallinity, and the ease of attachment onto some substrates (*e.g.*, Si substrate, stainless steel, Au foil).[1,9−11] In some cases, all three parameters have to be required simultaneously. Otherwise, it may lead to deterioration of the materials' native performances. For example, being a promising anodic material for lithium-ion batteries, Co_3O_4 properties have been explored extensively. However, in most cases, Co_3O_4 nanostructures are often mixed with carbon or other conductive polymers and compressed into pellets to enhance the system's conductivity and solidity.[4,12,13] Unfortunately, *via* this approach, it will definitely lead to the emergence of additional undesirable interfaces and defects, resulting in a denser structure which will lower the electron transfer velocities and electrolyte diffusion efficiency. Hence, the importance of growing free-standing one-dimensional (1D) nanostructures of Co_3O_4 with single-crystalline and mesoporous properties on the substrates has undoubtedly been realized, as they can conquer the above-mentioned drawbacks and improve the batteries' performance. However, due to the crystallographic nature of Co_3O_4 and its growth orientation, under most conditions, it is rather difficult to fabricate free-standing and well-aligned 1D nanostructures of Co_3O_4 on a variety of substrates, especially conducting substrates in solution. To date, reports involving this research area are few. Very recently, researchers reported a great achievement in Li-ion battery anodes from another transition metal oxide, V_2O_5, in which fairly high capacity and good capability were presented.[7] However, considering practical applications such as electric vehicles, which are the most

*Address correspondence to wang_yu@ices.a-star.edu.sg, lin_jianyi@ices.a-star.edu.sg.

Received for review September 21, 2009 and accepted February 02, 2010.

10.1021/nn9012675

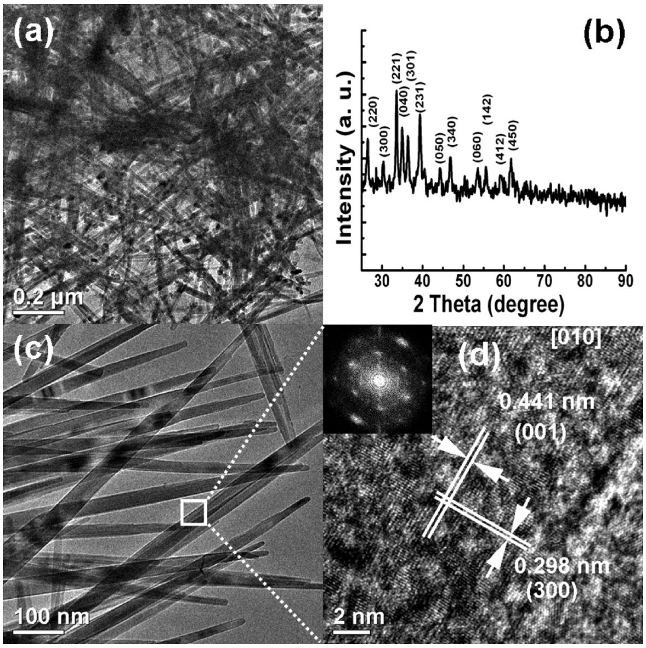

Figure 1. Low-magnification TEM image of $Co(CO_3)_{0.5}(OH)0.11H_2O$ nanobelts (a) and their corresponding XRD patterns (b) demonstrate that pure orthorhombic $Co(CO_3)_{0.5}(OH)0.11H_2O$ was obtainable in our experiments. The magnified TEM image (c) and the HRTEM image (d) reveal the nature of single-crystallinity in these nanobelts and the growth orientation of [100] for them. The inset in panel d is the corresponding FFT patterns.

promising means of transportation in the near future, the question researchers always ask is how to enhance the charge rate capability with high current surge while maintaining the specific capacity high enough and keeping the expenses low. This remains as a significant challenge even to today.

In this paper, one rational and facile method is introduced to fabricate a uniform and well-aligned $Co(CO_3)_{0.5}(OH)0.11H_2O$ nanobelt array on Ti foil, which is then converted into the nanobelt array of spinel Co_3O_4 *via* thermal treatment at 350 °C for 4 h. The Co_3O_4 nanobelt array exhibits combined properties of single-crystallinity and mesoporosity, revealing better conductivity and higher surface area compared to the normal nanoparticles in compressed bulk. Meanwhile, the nanobelt array exhibits wonderful contact with the conducting Ti foil, implying that this structure can be directly employed in practical applications, such as lithium-ion batteries and supercapacitors. In our Li-ion battery tests, the as-prepared Co_3O_4 nanobelt array exhibits a high capacity of 770 mAh/g under a considerably fast charge−discharge rate of 1.5C (1C is defined as one lithium per formula in an hour and, for Co_3O_4, 1C is equivalent to 111.1 mA/g) while stably maintaining a good capacity retention of more than 95%, even over 25 cycles in comparison with the discharge capacity of the second cycle. This is the first time that the Co_3O_4 nanobelt array has been successfully fabricated on Ti foil, and it also exhibits high capacity and good cyclability under the fast charge−discharge rate. Meanwhile, elaborate analyses show us an ultimate conclusion that our findings, showing the excellent performances in Li-ion battery testing, are closely associated with the unique structures and morphologies for our samples.

RESULTS AND DISCUSSION

From the representative transmission electron microscopy (TEM) images of the harvested samples in solution, it could be clearly detected that the samples exhibited uniform belt-shaped morphology (Figure 1a). Its corresponding X-ray diffraction (XRD) patterns showed that what we obtained was pure orthorhombic $Co(CO_3)_{0.5}(OH)0.11H_2O$ (Figure 1b) (JCPDS card No. 048-0083). By careful analysis, diffraction peaks were found to slightly shift to lower angles, and this may be due to the crystal expansion derived from samples' dimensions down to nanosize or from the equipment error. The locally magnified TEM image, as shown in Figure 1c, suggested these belt-shaped samples were 20−50 nm in width with needle-like tips, indicating they were characteristic of a preferentially one-dimensional growth along a specific direction. High-resolution TEM (HRTEM) analysis from the boxed area in Figure 1c showed two mutually vertical interplanes with lattice spaces of 0.298 and 0.441 nm, respectively, which matched very well with those of (300) and (001) crystal planes for orthorhombic $Co(CO_3)_{0.5}(OH)0.11H_2O$. The inset in Figure 1d showed the corresponding fast Fourier transformation (FFT) patterns, implying the single-crystalline nature of the samples. Furthermore, it could be deduced that the dominant growth orientation, which was also the nanobelt's axial direction, was fixed to be [100].

Further close observations from the TEM images showed that most nanobelts originated from dandelion-like bundles (Supporting Information). It was discovered that almost every bundle was interestingly composed of a number of nanobelts. Surprisingly, the nanobelts shared a common orientation and were strictly parallel to each other. The continuity of crystal lattices without any structural distortion or defects indicated that the whole bundle actually was single-crystalline in nature (Supporting Information). In fact, from the angle of crystal design and growth, this phenomenon provided one possibility of the oriented growth of well-aligned nanobelt arrays on some substrates, as long as crystal seeds could be formed on these substrates in advance.

Among materials that have been successfully synthesized by means of vertically aligned growth on certain substrates *via* wet-chemistry approach, ZnO is one of the most extensively studied. Generally, the formation of crystal seeds and nanostructured array growth took place in sequence with the reaction continuing in the same system without the addition of other reagents. The species of $Zn(OH)_4^{2-}$ or $Zn(NH_3)_4^{2+}$ as precursors of ZnO were formed during the first stage. ZnO crystal seeds developed from these species were then deposited onto the supporting substrates.[14−19] Motivated from these active seeds, ZnO nanowires or nanotubes developed and extended preferentially along the normal direction of the substrate, and the one-dimensional nanostructured array was finally fabricated. In our experiments, Co_3O_4 is a promising candidate for anodic materials of lithium-ion batteries and electrode materials for supercapacitors and has received intense research interests from all over the world. However, prior to the practical applications, one major barrier will have to be overcome, which is the problem of fabricating free-standing nanostructures of Co_3O_4 on conducting substrates. Furthermore, we aim to enhance the conductivity and diffusion efficiency of the electrolyte while spontaneously avoiding the substrates' interference because some substrates also have significant activities in lithium-ion battery testing (*e.g.*, Si wafer). However, metallic Ti is inert to Li-ion insertion and would be a good choice for Li-ion batteries' substrates. Acceptance of appropriate substrates for the aligned growth will be favorable for preventing the conducting substrates from being damaged by the electrolyte's corrosion and Li-ion insertion. Until now, there are still possibilities to venture into this research field.

From the above conclusions, it can be deduced that, if only orthorhombic $Co(CO_3)_{0.5}(OH)0.11H_2O$ crystal seeds were produced on the Ti foil, the subsequent growth of the nanobelt array would be feasible. Starting from this assumption, some experimental modifications had been made to the previous process of synthesizing $Co(CO_3)_{0.5}(OH)0.11H_2O$ nanobelt bundles. The concentrations of $Co(NO_3)_2$ and $NH_3 \cdot H_2O$ were increased a little to improve the crystallization of crystal seeds on the Ti foil. In the meantime, the Ti foil was tilted against the wall of the Teflon liner, with the interested surface facing down so as to effectively utilize the reflux of precursors and boost the liquid−solid interfacial crystallization process.

The color on the Ti foil surface changed from the original white to purple, indicating the samples had been successfully grown onto the Ti foil (Figure 2g). Upon treatment at 350 °C for 4 h, the surface color of Ti foil changed again from purple to black (Figure 2g). The visual changes not only presented the conversion of the samples' chemical compositions but also implied the changes in morphologies and crystal structures. XRD characterizations verified the conversion process, as demonstrated in Figure 2a,b. Figure 2a showed the XRD patterns collected from samples in their initial stage without any further treatment, except for rinsing with DI water and ethanol. The strongest peaks were ascribed to those of metallic Ti. However, the other peaks had been determined from orthorhombic $Co(CO_3)_{0.5}(OH)0.11H_2O$ after careful calibration. In comparison, Figure 2b exhibited totally different XRD patterns with the exception of Ti diffraction peaks, and these patterns could be undoubtedly indexed as spinel Co_3O_4. Under our experimental conditions, Ti foil with dimensions up to 1 × 3 cm could be uniformly coated with the samples (Supporting Information). In actual demonstrations and characterizations, the foils were normally divided into even smaller pieces prior to usage rather than being applied directly (Figure 2g). A typical scanning electron microscope (SEM) image of the orthorhombic $Co(CO_3)_{0.5}(OH)0.11H_2O$ nanobelt array is presented in Figure 2c, while the corresponding SEM image of samples experiencing subsequent calcinations is shown in Figure 2d. From both of the images, it can be clearly detected that the as-synthesized samples exhibit smooth morphologies in a micrometric scale. From the enlarged SEM images shown in Figure 2e,f, we could unanimously infer that the samples were still maintaining the uniform nanobelt array after calcinations (Figure 2f) compared to that before calcinations (Figure 2e). An individual nanobelt presented regular grass-blade-shaped morphology stemming from the bottom section and eventually developed into one inseparable part of a nanobelt bundle (Figure 2e,f,h). By careful observations, we can draw a conclusion that these nanobelts among the bundle originated from the same starting point and grew along the common direction, as certified in Figure 2h, which almost was along the direction vertical to surface of the Ti foil. Because of the nanobelt's "grass-blade" morphology, leading to a deviation of barycenter from its axial orientation, it was hard to extend its "stem" along a fixed direction. This shed light on why most of the samples deviated a little from the normal direction that is perpendicular to the Ti foil surface (Figure 2e,f). Furthermore, it is noteworthy that our samples were remarkably sticky to the substrate. Even after strong ultrasonication over 3 min, no samples would apparently be peeled off from the substrate, implying a strong contact between them. To the best of our knowledge, this is the first time that a finding of such an achievement is reported, where a thoroughly nonhomologous material with nanobelt morphology was grown directly on Ti foil *via* a wet-chemistry approach. Since it is more difficult to synthesize nanobelts than nanowires and nanorods,[20] few reports have been involved in the preparation of nanobelt arrays on substrates, inclusive of using chemical vapor deposition (CVD) methods.

In our synthesis, $Co(CO_3)_{0.5}(OH)0.11H_2O$ was first detected to exhibit the property of one-dimensional preferential growth originating from the common crystal seeds. The assumption given before was that, provided some crystal seeds could be formed on some substrates beforehand, the following oriented growth of $Co(CO_3)_{0.5}(OH)0.11H_2O$ would definitely have resulted in the nanobelt array on the substrates. In our experiments, Ti foil was applied to fulfill the assumption for the sake of two important specialties. First, the required

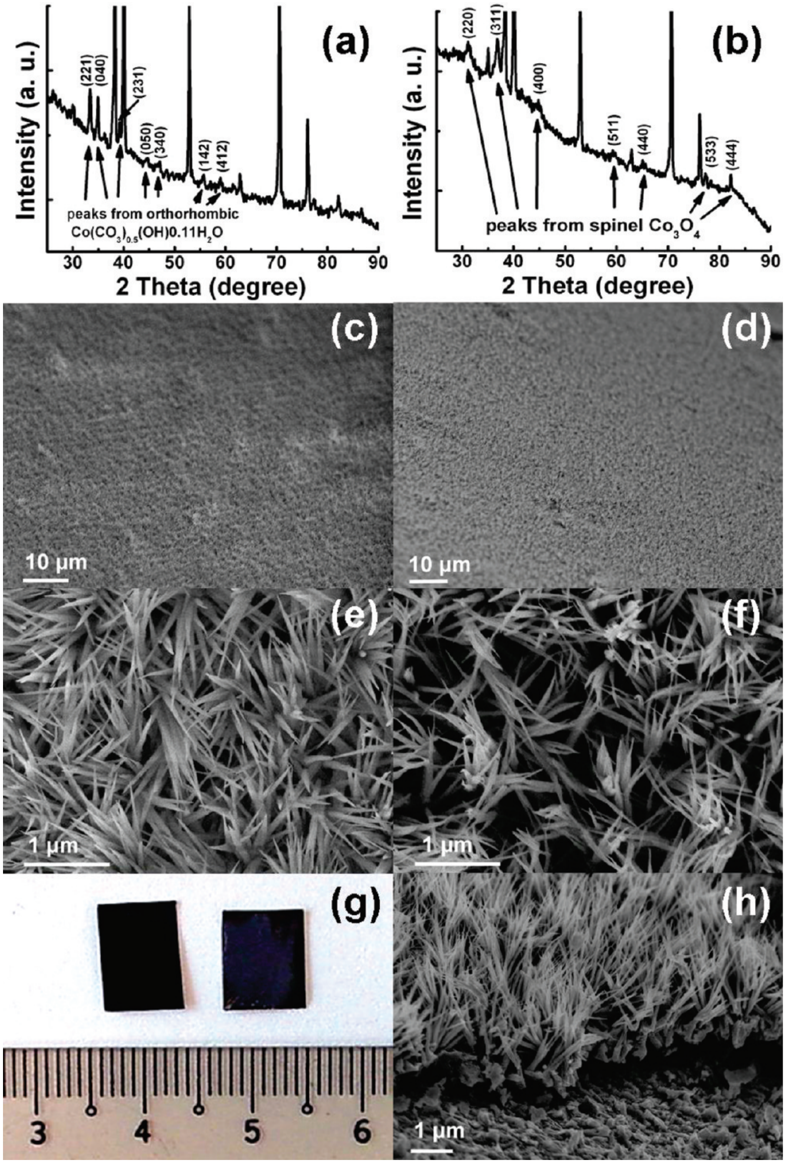

Figure 2. XRD patterns collected from $Co(CO_3)_{0.5}(OH)0.11H_2O$ (a) and Co_3O_4 (b) nanobelt array attached to Ti foil. (c) Low-magnification SEM image and (e) locally enlarged image. In comparison, the SEM images for the corresponding Co_3O_4 nanobelt array on Ti foil are exhibited in panels d and f in sequence. (g) Optical picture with a ruler in millimeter scale as the background for $Co(CO_3)_{0.5}(OH)0.11H_2O$ (right panel) and Co_3O_4 (left panel). From the side view of the Co_3O_4 nanobelt array on Ti foil (h), it can be detected that these nanobelts developed from the Ti foil and exhibited good contact with the substrate.

substrates should be significantly resistant to the corrosion from the electrolyte in lithium-ion batteries and also be conducting, so that charge transfer occurring during the period of charge−discharge would take place. Second, Ti foil generally was coated with a thin layer of TiO_2. This TiO_2 layer would be covered with a number of hydroxyl groups while immersed in basic solution due to its isoelectric point with a pH value of 4.5−6.5,[21] especially in the strong basic solution over high temperature. These dangling hydroxyl groups atomically stick onto the substrate and act as "hunters" through hydrogen bonding to capture the originally formed $Co(CO_3)_{0.5}(OH)0.11H_2O$ crystal seeds. The fluctuant and textured surface of the TiO_2 layer was also favorable for entrapping and solidifying the tiny $Co(CO_3)_{0.5}(OH)0.11H_2O$ crystal seeds.[22,23] As demonstrated, the final results confirmed our assumption. The synthetic mechanism and procedure are described in Scheme 1. On the basis of the above assumptions and results, fabrication of the $Co(CO_3)_{0.5}(OH)0.11H_2O$ nanobelt array may be extended to other similar substrates such as silicon wafer.

As a chemically unstable material, $Co(CO_3)_{0.5}(OH)0.11H_2O$ is easily converted to Co_3O_4, which is another functional material. After calcinations at 350 °C for 4 h, the Co_3O_4 nanobelt array had been obtained and verified from SEM and XRD characterizations (Figure 3). The products were peeled off from the supporter and collected for HRTEM, XRD examinations, and Brunauer−Emmett−Teller (BET) nitrogen adsorp-

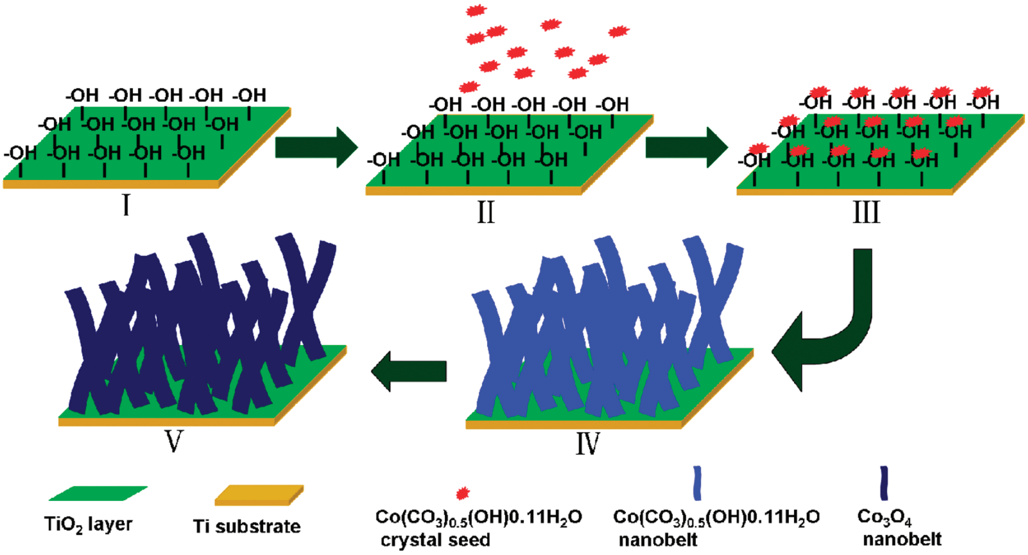

Scheme 1. Schematic illustration for the whole synthetic procedure: Basically, Ti foil is covered with a thin TiO$_2$ layer because of metallic titanium's oxidation in normal atmosphere. Experiencing immersion into strong basic solution, especially over high temperature (170 °C), hydrophilic groups of hydroxyl will be formed on the surface of the TiO$_2$ layer (I). During the initial stage of reaction, some earlier formed crystal seeds of Co(CO$_3$)$_{0.5}$(OH)0.11H$_2$O will be adsorbed onto the surface with function of hydrogen bonding (II and III). Starting from these active centers, Co(CO$_3$)$_{0.5}$(OH)0.11H$_2$O nanobelts will be developing and finally be formed into nanobelt array (IV). Owing to the chemical instability of Co(CO$_3$)$_{0.5}$(OH)0.11H$_2$O and the tendency to be decomposed when exposed to thermal environment, the Co(CO$_3$)$_{0.5}$(OH)0.11H$_2$O nanobelt array easily turns into a mesoporous Co$_3$O$_4$ nanobelt array with essence of single-crystallinilty (V) after calcinations under 350°C for 4 h.

tion and desorption isotherm measurement. Figure 3a exhibited a typical TEM image, from which we could clearly detect some belt-shaped structures with some distinct mesopores on the surface. The locally enlarged HRTEM image in Figure 3b showed two hexagonally crossing interdistances of 0.285 and 0.283 nm, indicating that the directly exposed crystal plane open to us was (1$\bar{1}$1), combined with its corresponding FFT patterns shown in the inset of Figure 3b. Figure 3b shows some observations of mesopores with diameters of ap-

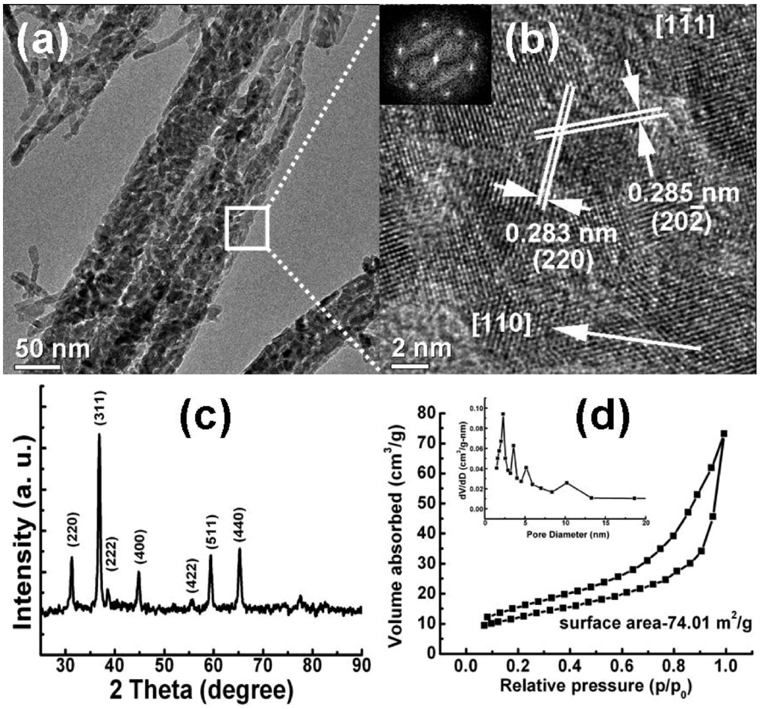

Figure 3. Upon calcinations at 350 °C for 4 h, Co(CO$_3$)$_{0.5}$(OH)0.11H$_2$O nanobelts are converted to mesoporous Co$_3$O$_4$ nanobelts (a). From the rectangular area marked in panel a, HRTEM image (b) reveals well-crystallized Co$_3$O$_4$, where some mesopores are dispersed inside, and meanwhile implies single-crystallinity for the samples. XRD (c) and BET (d) diagrams, proving the good crystallization and high surface area for our samples. The inset in panel d is the pore size distribution, centered at 2.4 nm.

proximately 2.4 nm. Further characterizations, including XRD (Figure 3c) and BET (Figure 3d), were presented to certify that the products under calcinations were mesoporous spinel Co_3O_4 (JCPDS No. 74-1657) with a surface area of 74.01 m^2/g and a pore size centered at 2.4 nm (inset of Figure 3d). In fact, the property of mesoporosity could be reasonably deduced from the relief of H_2O and CO_2 through $Co(CO_3)_{0.5}(OH)0.11H_2O$ thermal decomposition. More interestingly, the presence of mesoporosity did not affect the crystalline continuity at all (Figure 3b). Thus, it was inferred from the above investigations that what we harvested after calcinations was a single-crystal Co_3O_4 nanobelt array with characteristics of mesoporosity. Besides being single-crystal in nature and having a rather large surface area, the intensive contact with the substrate made our products a potential candidate for the anodic materials of lithium-ion batteries.

Figure 4 shows the electrochemical performance of the as-synthesized Co_3O_4 naonbelt array. Figure 4a was the voltage capacity profile associated with charge−discharge rate of 1.5C based on the Co_3O_4/Li half cell (equivalent to 177 mA/g). From the first discharge curve, it was observed that there was one distinct plateau located at 1 V and the other unclear plateau at 1.3 V, which corresponded to the reduction processes of CoO to Co and Co_3O_4 to CoO, respectively.[4,24,25] Generally, the detection of a plateau in high voltage was scarcely reported, except samples with high surface area or very low testing current density applied.[24,25] For our samples, a high surface area of 74.01 m^2/g was recorded, but the testing current density was as high as 177 mA/g, which was comparable to a previous report,[2] where the surface area was as low as 7.6 m^2/g. Starting from this point, whether there was the existence of a discharge plateau or not at high voltage (1.3 V) could be understandable. The discharge capacity of the first cycle was approximately 1086.1 mAh/g, which was even higher than that of the theoretical capacity for Co_3O_4 (890 mAh/g). According to the previously reported results,[5,26] it could be attributed to the irreversible reactions (*e.g.*, electrolyte decomposition occurring during the first discharge cycle). Then irreversible capacity loss of 330 mAh/g in the second cycle frequently occurred in the anode materials.[1,2] The subsequent charging processes displayed the standard voltage hysteresis, signifying the conversion reaction mechanism.[4,12] Afterward, the following charge−discharge curves tended to be stable, implying that the electrochemical reactions were proceeding into the cyclable stages.

Figure 4b shows the discharge capacities *versus* cycle number at a rate of 1.5C for the Co_3O_4 nanobelt array. The samples exhibited improved reversible discharge capacities over 25 cycles. More interestingly, the discharge capacities from the second cycle gradually increased rather than decreased. The maximum discharge capacity could reach up to 788.7 mAh/g, which corresponded to 88.6% of the theoretical capacity for Co_3O_4. To the best of our knowledge, this is the best result reported for Co_3O_4 under such a high discharge rate without the addition of any other ancillary materials (binder and carbon black). In comparison, nanoparticles of Co_3O_4 with sizes of 10−15 nm had been utilized to investigate the electrochemical properties (Supporting Information). As shown in Figure 4b, it was observed

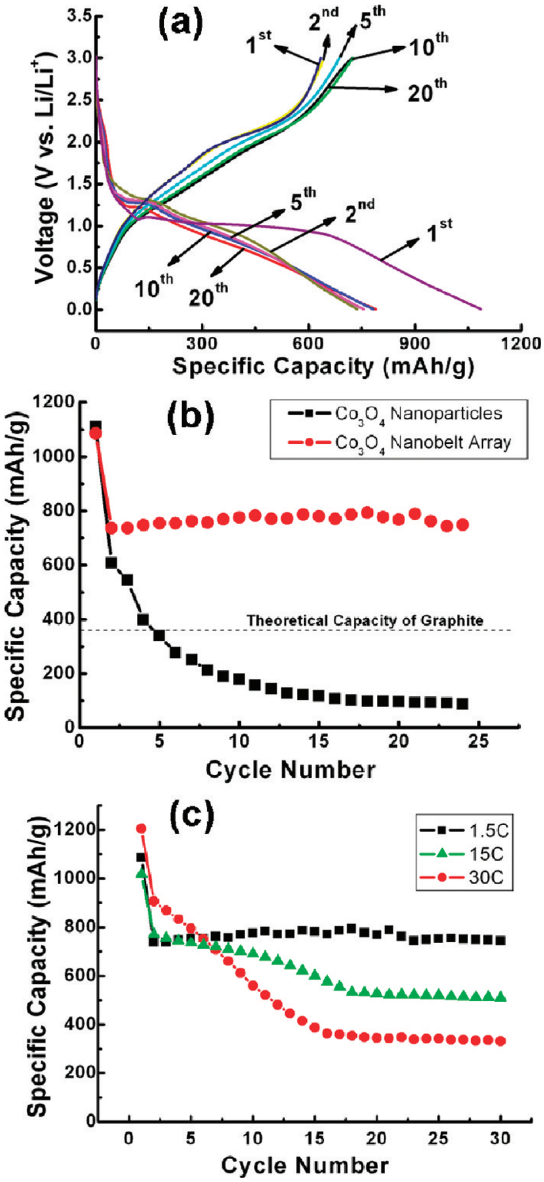

Figure 4. Voltage-specific capacity profiles are presented in panel a, revealing the distinct discrepancy between the first cycle and the subsequent cycles. The diagrams of specific capacity *versus* cycle number (b) derived from the Co_3O_4 nanobelt array on Ti foil (red) and Co_3O_4 nanoparticles (black) show us the high capacity and prominent cyclability for the Co_3O_4 nanobelt array. When the discharge rates are increased to 15 and 30C, the specific capacities will drop to 530 mAh/g (c, green) and 320 mAh/g (c, red), respectively. However, the high capacities still could be retained over 15 cycles until 30 cycles under the ultrahigh discharge rates, implying the excellent rate capabilities for our samples. The black dots in panel c are the data collected at the discharge rate of 1.5C as a comparison.

that within five cycles, their discharge capacities decayed to 372 mAh/g, which was close to the theoretical capacity of graphite, and rapidly faded below 100 mAh/g. Why was there such a large discrepancy between the two systems? The only possible explanation could be attributed to the unique morphology and structure for our synthesized Co_3O_4 nanobelt array. The improved performance was determined to originate from five advantages for our samples: (1) Free-standing structure was favorable for electron transportation and the insertion and extraction of lithium ions because Co_3O_4 nanobelts sticked tightly to the conducting substrate, building up an expressway for charge transfer. The loose texture and enormous space among the individual nanobelts provided a higher efficiency of lithiation and delithiation under the aid of electrolyte penetration. Definitely, it was also ideal for the accommodation of large volume changes during reactions. (2) High specific surface area, especially with a large quantity of hydrophilic groups of hydroxyl exposed outside,[27] effectively improved the electrical contact and lithium absorption during electrochemical reactions, similar to SnO_2.[28] (3) Even smaller widths of 20−40 nm for our nanobelts would definitely increase the efficiency of lithiation and delithiation. It also shortened the charge transfer pathway and lowered the exchange resistance for Li ions between electrolyte and functional materials.[5] (4) Elastic feature of nanobelts released the pressure imposed on them while assembling cells and prevented the nanobelt array from pulverization and fragmentation (Supporting Information). (5) Specific structure consisting of needle-like Co_3O_4 tips with lengths limited to 2−3 μm promoted electrolyte diffusion. All those above would undoubtedly improve the battery's performance.

By imposing much higher discharge rates of 15C (1670 mA/g) and 30C (3350 mA/g) on the Co_3O_4 nanobelt array, we would investigate their rate capability properties. In Figure 4c, it was clearly observed that, after no less than 30 cycles, the specific capacities steadily delivered 530 mAh/g when cycled at a rate of 15C and 320 mAh/g at 30C. Compared to the previously reported results, the enhanced performance for our samples could be attributed to their unique morphology and structure. Maintaining rather high specific capacities while experiencing ultrahigh discharge rates further validated our samples to be promising candidates for some practical applications where a large amount of stored charges was required, such as electric vehicles and portable electronic devices. The prominent rate capability determined in our experiments was ideal for such applications.

CONCLUSION

In summary, it was described in this paper that based on the elaborate analyses of the qualification of growing well-aligned and one-dimensional nanostructures on the substrates, and combined with the structural analyses of $Co(CO_3)_{0.5}(OH)0.11H_2O$ nanobelt synthesis, the Co_3O_4 nanobelt array had been rationally synthesized on Ti foil. This result not only enriched the contents of the oriented growth of 1D nanostructured materials on some applicable substrates but also showed us an illustration of the rationally designed synthesis of well-aligned, functional, and technically important materials. These Co_3O_4 nanobelts spontaneously exhibited mesoporosity and large surface areas, which were attributed to the thermal decomposition of $Co(CO_3)_{0.5}(OH)0.11H_2O$. It was revealed from Li-ion battery tests that the obtained samples displayed wonderful specific capacities and rate capabilities, arising from their unique hierarchical structures. The Co_3O_4 nanobelt array may possibly be directly applied in some practical applications without the requirement of adding any other ancillary materials.

MATERIALS AND METHODS

Materials: All chemicals or materials were used directly without any further purification prior to usage. Ethylene glycol (Fisher Chemical, 99.99%), ammonia hydroxide ($NH_3 \cdot H_2O$, 28−30 wt %, J.T. Baker), cobalt nitrate ($Co(NO_3)_2$, 99.9%, Aldrich), sodium carbonate (Na_2CO_3, 99.9%, Aldrich), and titanium foil (0.127 mm (0.005 in.) thick, annealed, 99%, Alfa Aesar), metallic Li foil (99.9%, Aldrich) were used.

Synthesis of $Co(CO_3)_{0.5}(OH)0.11H_2O$ Nanobelts: In a typical synthesis, 20 mL of ethylene glycol, 12.5 mL of concentrated $NH_3 \cdot H_2O$ (28 wt ratio %), 1 mL of 1 M Na_2CO_3 aqueous solution, and 5 mL of 1 M Co $(NO_3)_2$ aqueous solution were mixed step-by-step under vigorous stirring with intervals of 2 min. After that, another 20 min was introduced into the stirring period, and finally, the mixture turned into a homogeneous solution with a deep dark color. Once the precursor was transferred into a Teflon-lined stainless steel autoclave with a volume of 45 mL, a thermal treatment was performed for the Teflon liner in an electric oven at 170 °C for 16 h. After the autoclave was cooled naturally to room temperature in a fumehood, samples deposited at the bottom were collected and washed by centrifugation for at least three cycles using deionized water (DI water) and one cycle using pure ethanol. The as-synthesized samples were then dried in a vacuum oven at 40 °C overnight to remove the absorbed water for the subsequent characterizations. Generally, 300−400 mg samples could be produced from the synthesis (Supporting Information).

Synthesis of $Co(CO_3)_{0.5}(OH)0.11H_2O$ Nanobelt Array on Ti Foil and the Conversion to Co_3O_4 Nanobelt Array: Prior to the synthesis, a Ti foil with a size of 1 × 3 cm was rinsed with DI water and pure ethanol subsequently or sonically cleaned by a mixture of DI water, ethanol, and acetone with a volume ratio of 1:1:1 for 10 min. Afterward, the Ti foil was tilted against the wall of the autoclave at a certain angle, with the interested surface facing down. A little modified solution composed of ethylene glycol, concentrated $NH_3 \cdot H_2O$ (28 wt %), 1 M Na_2CO_3 aqueous solution, and 1 M Co $(NO_3)_2$ aqueous solution was slowly poured into the autoclave. The autoclave was then tightly sealed and left in an oven at 140−170 °C for 16−64 h for reaction. Once the reaction was over, the Ti foil was taken out and dried in a vacuum oven at 40 °C for at least 3 h. In the event of the conversion from $Co(CO_3)_{0.5}(OH)0.11H_2O$ nanobelt to Co_3O_4, another thermal treatment was performed at 350 °C for 4 h with a heating ramp of 1

°C/min until the products' color changed from pink or purple to black.

Characterization of the Samples: Scanning electron microscopy (SEM, FEI, 5 kV), transmission electron microscopy (TEM, Philips, Tecnai, F20, 200 kV), power X-ray diffraction (XRD, Bruker D8 Advance X-ray diffractometer with Cu Kα radiation), and Brunauer−Emmett−Teller surface area measurement (BET, Quantachrome Autosorb-6B surface area and pore size analyzer) were applied to characterize the obtained samples.

Electrochemical Characterization: Prior to actual testing, Ti foil with samples of 0.6−0.9 mg/cm^2 covered was first cut into smaller pieces with a size of 6 $\times$ 6 mm and weighed in a high-precision analytical balance (Sartorius, max weight 5100 mg, $d = 0.001$ mg). The obtained pieces of Ti were then used as electrodes with 1 M $LiPF_6$ in ethylene carbonate and diethyl carbonate (EC-DEC, v/v = 1:1) as electrolyte. Celgard 2400 was used as the separator film to isolate the two electrodes. Pure Li foil (99.9%, Aldrich) was accepted to server as counter electrode and reference electrode. The cell was assembled in an argon-filled glovebox where moisture and oxygen concentrations were strictly limited to below 1 ppm. The electrochemical tests were performed on Neware Battery Testing System in a model 5 V1 mA. After testing, the tested Co_3O_4 nanobelt array was removed from the Ti foil by knife and the Ti foil was completely cleaned by ultrasonication subsequently and then weighed in the analytical balance again. Through this way, the exact sample mass used for Li-ion battery testing was available.

Acknowledgment. We acknowledge financial support from Intelligent Energy Distribution Systems (IEDS) of Agency for Science, Technology, and Research (ASTAR) in Singapore. Y.W. would like to express his appreciation to H.J. Zhang, P.S. Ludger, and K.S. Martin for their help during the paper's preparation.

Supporting Information Available: Schematic illustration for the sample's structural advantage in cell assembly, detailed TEM analyses on sample's 1-D preferential growth, optical pictures for samples, and TEM image for Co_3O_4 nanoparticles. This material is available free of charge *via* the Internet at http://pubs.acs.org.

REFERENCES AND NOTES

1. Kim, M. G.; Cho, J. Reversible and High-Capacity Nanostructured Electrode Materials for Li-Ion Batteries. *Adv. Funct. Mater.* **2009**, *19*, 1497–1514.
2. Lou, X. W.; Deng, D.; Lee, J. Y.; Feng, J.; Archer, L. A. Self-Supported Formation of Needlelike Co_3O_4 Nanotubes and Their Application as Lithium-Ion Battery Electrodes. *Adv. Mater.* **2008**, *20*, 258–262.
3. Zhan, F. M.; Geng, B. Y.; Guo, Y. J. Porous Co_3O_4 Nanosheets with Extraordinarily High Discharge Capacity for Lithium Batteries. *Chem.—Eur. J.* **2009**, *15*, 6169–6174.
4. Poizot, P.; Laruelle, S.; Grugeon, S.; Dupont, L.; Tarascon, J. M. Nano-Sized Transition-Metal Oxides as Negative-Electrode Materials for Lithium-Ion Batteries. *Nature* **2000**, *407*, 496–499.
5. Nam, K. T.; Kim, D. W.; Yoo, P. J.; Chiang, C. Y.; Meethong, N.; Hammond, P. T.; Chiang, Y. M.; Belcher, A. M. Virus-Enabled Synthesis and Assembly of Nanowires for Lithium Ion Battery Electrodes. *Science* **2006**, *312*, 885–888.
6. Xiong, S. L.; Yuan, C. Z.; Zhang, X. G.; Xi, B. J.; Qian, Y. T. Controllable Synthesis of Mesoporous Co_3O_4 Nanostructures with Tunable Morphology for Application in Supercapacitors. *Chem.—Eur. J.* **2009**, *15*, 5320–5326.
7. Liu, J.; Xia, H.; Xue, D. F.; Lu, L. Double-Shelled Nanocapsules of V_2O_5-Based Composites as High-Performance Anode and Cathode Materials for Li Ion Batteries. *J. Am. Chem. Soc.* **2009**, *131*, 12086–12087.
8. Yu, Y.; Gu, L.; Wang, C. L.; Dhanabalan, A.; Aken, P. A.; van; Maier, J. Encapsulation of Sn@Carbon Nanoparticles in Bamboo-like Hollow Carbon Nanofibers as an Anode Material in Lithium-Based Batteries. *Angew. Chem., Int. Ed.* **2009**, *48*, 6485–6489.
9. Reddy, A. L. M.; Shaijumon, M.; Gowda, S. R.; Ajayan, P. M. Coaxial MnO_2/Carbon Nanotube Array Electrodes for High-Performance Lithium Batteries. *Nano Lett.* **2009**, *9*, 1002–1006.
10. Park, M. S.; Wang, G. X.; Kang, Y. M.; Wexler, D.; Dou, S. X.; Liu, H. K. Preparation and Electrochemical Properties of SnO_2 Nanowires for Application in Lithium-Ion Batteries. *Angew. Chem., Int. Ed.* **2007**, *46*, 750–753.
11. Chan, C. K.; Peng, H. L.; Liu, G.; Warth, K. M.; Zhang, X. F.; Huggins, R. A.; Cui, Y. High-Performance Lithium Battery Anodes Using Silicon Nanowires. *Nat. Nanotechnol.* **2008**, *3*, 31–35.
12. Taberna, P. L.; Mitra, S.; Poizot, P.; Simon, P.; Tarascon, J. M. High Rate Capabilities Fe_3O_4-Based Cu Nano-Architectured Electrodes for Lithium-Ion Battery Applications. *Nat. Mater.* **2006**, *5*, 567–573.
13. Li, Y. G.; Tan, B.; Wu, Y. Y. Mesoporous Co_3O_4 Nanowire Arrays for Lithium Ion Batteries with High Capacity and Rate Capability. *Nano Lett.* **2008**, *8*, 265–270.
14. Tian, Z. R.; Voigt, J. A.; Liu, J.; Mckenzie, B.; Mcdermott, M. J. Biomimetic Arrays of Oriented Helical ZnO Nanorods and Columns. *J. Am. Chem. Soc.* **2002**, *124*, 12954–12955.
15. Vayssieres, L. Growth of Arrayed Nanorods and Nanowires of ZnO from Aqueous Solutions. *Adv. Mater.* **2003**, *15*, 464–466.
16. Greene, L. E.; Law, M.; Tan, D. H.; Montano, M.; Goldberger, J.; Somorjai, G.; Yang, P. D. General Route to Vertical ZnO Nanowire Arrays Using Textured ZnO Seeds. *Nano Lett.* **2005**, *5*, 1231–1236.
17. Li, Q. C.; Kumar, V.; Li, Y.; Zhang, H. T.; Marks, T. J.; Chang, R. P. H. Fabrication of ZnO Nanorods and Nanotubes in Aqueous Solutions. *Chem. Mater.* **2005**, *17*, 1001–1006.
18. Vayssieres, L.; Keis, K.; Hagfeldt, A.; Lindquist, S. E. Three-Dimensional Array of Highly Oriented Crystalline ZnO Microtubes. *Chem. Mater.* **2001**, *13*, 4395–4398.
19. Li, W. J.; Shi, E. W.; Zhong, W. Z.; Yin, Z. W. Growth Mechanism and Growth Habit of Oxide Crystals. *J. Cryst. Growth* **1999**, *203*, 186–196.
20. Pan, Z. W.; Dai, Z. R.; Wang, Z. L. Nanobelts of Semiconducting Oxides. *Science* **2001**, *291*, 1947–1949.
21. Lee, H. S.; Hur, T.; Kim, S.; Kim, J. H.; Lee, H. I. Effects of PH and Modification of TiO_2 with SiO_x on the Photocatalytic Degradation of a Pyrimidine Derivative. *Catal. Today* **2003**, *84*, 173–180.
22. Gouldstone, A.; Van Vliet, K. J.; Suresh, S. Simulation of Defect Nucleation in a Crystal. *Nature* **2001**, *411*, 656.
23. Formo, E.; Camargo, P. H. C.; Lim, B. M.; Jiang, J.; Xia, Y. N. Functionalization of ZrO_2 Nanofibers with Pt Nanostructures: The Effect of Surface Roughness on Nucleation Mechanism and Morphology Control. *Chem. Phys. Lett.* **2009**, *476*, 56–61.
24. Larcher, D.; Sudant, G.; Leriche, J. B.; Chabre, Y.; Tarascon, J. M. The Electrochemical Reduction of Co_3O_4 in a Lithium Cell. *J. Electrochem. Soc.* **2002**, *149*, A234–A241.
25. Li, W. Y.; Xu, L. N.; Chen, J. Co_3O_4 Nanomaterials in Lithium-Ion Batteries and Gas Sensors. *Adv. Funct. Mater.* **2005**, *15*, 851–857.
26. Shaju, K. M.; Jiao, F.; Debar, A.; Bruce, P. G. Mesoporous and Nanowire Co_3O_4 as Negative Electrodes for Rechargeable Lithium Batteries. *Phys. Chem. Chem. Phys.* **2007**, *9*, 1837–1842.
27. Binni, V; Teo, C. H.; Zhu, Y. W.; Mogalahalli, V. R.; Bobba, V. R. C.; Andrew, T. S. W.; Tan, B. C. V.; Lim, C. T.; Sow, C. H. Co_3O_4 Nanostructures with Different Morphologies and Their Field-Emission Properties. *Adv. Funct. Mater.* **2007**, *17*, 1932–1939.
28. Lou, X. W.; Deng, D.; Lee, J. Y.; Archer, L. A. Preparation of SnO_2/Carbon Composite Hollow Spheres and Their Lithium Storage Properties. *Chem. Mater.* **2008**, *20*, 6562–6566.